Available online at www.sciencedirect.com
SCIENCE DIRECT®
Thin Solid Films 431–432 (2003) 262–266
thin solid films
www.elsevier.com/locate/tsf

Structural and chemical interface characterization of CdTe solar cells by transmission electron microscopy

M. Terheggen[a,*], H. Heinrich[a], G. Kostorz[a], A. Romeo[b], D. Baetzner[b], A.N. Tiwari[b], A. Bosio[c], N. Romeo[c]

[a]*ETH Zurich, Institute of Applied Physics, CH-8093 Zurich, Switzerland*
[b]*ETH Zurich, Laboratory for Solid State Physics, Thin Film Physics Group, Technopark, ETH Building, Technoparkstr.1, CH-8005 Zurich, Switzerland*
[c]*Department of Physics, University of Parma, I-43100 Parma, Italy*

Abstract

CdTe/CdS thin film solar cells have been grown by high-vacuum evaporation (HVE) and close-space sublimation. To understand the role of Cl on the microstructure and composition of the CdTe/CdS layers and interfaces, the cells were annealed for different durations after different amounts of $CdCl_2$ had been deposited. Transmission electron microscopy shows a loss of orientational relationship between CdTe and CdS after annealing under the influence of Cl. The interdiffusion of S and Te across the interface is measured quantitatively and segregation of Cl, Te and O at the CdTe/CdS interface is detected by energy-dispersive X-ray mapping in the electron microscope. The results show a strong correlation with the diffusion of Cl along the CdTe grain boundaries, which is directly proved for the first time. It is suggested that recrystallization of CdTe grains starts from the CdTe surface and proceeds towards the interface. Cells grown by HVE show all the features expected from the predominance of recrystallization.

Keywords: Solar cells; CdTe; $CdCl_2$; Transmission electron microscopy

1. Introduction

CdTe has a high potential as a thin film solar cell absorber on an industrial level [1]. Efficiencies of 7–10% have been obtained on large area modules. But grain boundaries and interfacial defects remain the main limitation for improvement of the efficiency of CdTe/CdS cells, since both influence the photo current. An annealing treatment after deposition of $CdCl_2$ on the CdTe layer improves the cell efficiency and hence has been intensively studied, see e.g. [2]. Modelling of photo currents has helped to link the electrical performance of CdTe/CdS solar cells to their structure and composition [3]. However, little is known on the diffusion mechanism of Cl in CdTe and on the structural features and distribution of chemical species on the nanometer or atomic scale. Therefore, analytical high-resolution transmission electron microscopy (TEM) has been used to obtain structural and chemical information on the changes induced by the $CdCl_2$ treatment. Results on the diffusion of Cl in CdTe, segregation at the CdTe/CdS interface and reductions of internal stress and defect densities at the interface and in bulk CdTe are presented.

2. Experimental details

The TEM studies were performed using a Philips CM30 electron microscope equipped with an energy-dispersive X-ray spectroscopy (EDS) detector, and a Tecnai F30 electron microscope equipped with a Gatan Imaging Filter for energy-filtered TEM (EFTEM). To compare the influence of different growth methods and temperatures, CdTe absorber layers were deposited by high-vacuum evaporation (HVE) as well as close-space sublimation (CSS). For HVE-grown cells, CdS layers approximately 700 nm thick were grown at a substrate temperature of 150 °C by use of HVE onto SnO_x:F-

*Corresponding author. Tel.: +41-1-6332142; fax: +41-1-6331105.
E-mail address: terheggen@iap.phys.ethz.ch (M. Terheggen).

0040-6090/03/$ - see front matter © 2003 Elsevier Science B.V. All rights reserved.
doi:10.1016/S0040-6090(03)00268-2

Table 1
Deposition and $CdCl_2$ treatment details of the samples

Sample	$CdCl_2$ (nm)	Time (min) At temperature (°C)	Deposition
1	0	As deposited	HVE
2	400	30 at 430 in Air	HVE
3	150	30 at 430 in Air	HVE
4	70	30 at 430 in Air	HVE
5	0	30 at 430 in Air	HVE
6	400	6 at 430 in Air	HVE
7	400	11 at 430 in Air	HVE
8	0	As deposited	CSS
9	l00	15 at 420 in Ar + Air	CSS

coated soda-lime glass (SLG) substrates. A layer of CdTe with a thickness of 3 μm was deposited by means of HVE at a substrate temperature of 150 or 300 °C. The CSS-grown cells consist of a sputtered CdS layer of a thickness of 100 nm on SnO_x:F-covered SLG. The CdS layer is annealed in air at 500 °C for 30 min prior to the CdTe deposition at 520 °C. Both types of cell are submitted to different $CdCl_2$ treatments under the conditions listed in Table 1. The HVE-deposited cells show a maximum efficiency of 12.4% with a short-circuit current density of 23 mA/cm^2 and an open-circuit voltage of 800 mV. For TEM studies, cross-sectional samples were prepared by mechanical cutting and polishing, dimple grinding and ion milling. For determination of the lattice parameters and of absolute concentrations, $Cd_{50}S_xTe_{50-x}$ polycrystals with $x=5$ and 45 were prepared as standards from CdS and CdTe in a furnace at 1150 °C. The homogeneity and composition were verified with analytical TEM.

3. Experimental results and discussion

3.1. Structural changes

An interface in as-deposited CdTe/CdS (HVE) is shown in the high-resolution micrograph of Fig. 1A with the CdTe layer in [1-1 0] and the CdS layer in [2-1-1 0] orientation. Frequent changes in the stacking sequence between one of the two twin variants of the cubic structure (a or b) or hexagonal stacking sequences (c) in CdTe indicate a low stacking-fault energy. These changes in stacking sequence and the lattice mismatch between CdTe and CdS are reflected in Fig. 1B, the fast Fourier transform of Fig. 1A. The polymorphic CdTe shows long streaks, characteristic of stacking defects of the (1 1 1) planes, while the lattice mismatch is reflected by the different distances between diffraction spots of the CdS (0 0 0 2) planes and the streaks of the CdTe (1 1 1) planes. However, the orientational relationship between CdTe and CdS after deposition is obvious as both structures show a preferred [1 1 1] orientation perpendicular to the interface in Fig. 1A and B. Fig. 1C shows a high-resolution structural image of the interface after $CdCl_2$ treatment. Here the orientational relationship between CdTe and CdS is lost, and random orientational relations result between the CdTe (1 1 0) planes and the CdS (0 0 0 1) planes, both relative to each other and in relation to the interface. Note that Fig. 1C and D show closely similar orientations of CdTe and CdS which allow for the observation of both lattices with atomic resolution. The CdTe [l-1 0] and the CdS [2-1 1 0] poles are still parallel. This is not the general case, in which no special orientation relationship between CdTe and CdS can be found after $CdCl_2$ treatment [4]. The recrystallized CdTe grains are characterized by a reduced stacking-fault density. The microstructure contains essentially one cubic twin variant, and well defined diffraction spots are seen in Fig. 1D instead of streaks. Simple grain growth starting from columnar CdTe grains, all with similar [1 1 1] orientation perpendicular to the interface, would not result in a loss of orientational relationship between CdTe and CdS but would rather lead to grains of larger size with the CdTe (1 1 0) planes still parallel to the interface. For comparison, sample 5 was annealed without Cl and shows only grain growth, but no change in crystallographic orientation. A smaller increase of the grain size and less reduction in stacking fault density than with $CdCl_2$ are observed, but there is no loss of texture. CSS-deposited samples (8 and 9) show similar effects, but, exhibiting larger grains after deposition, both the increase in grain size and the

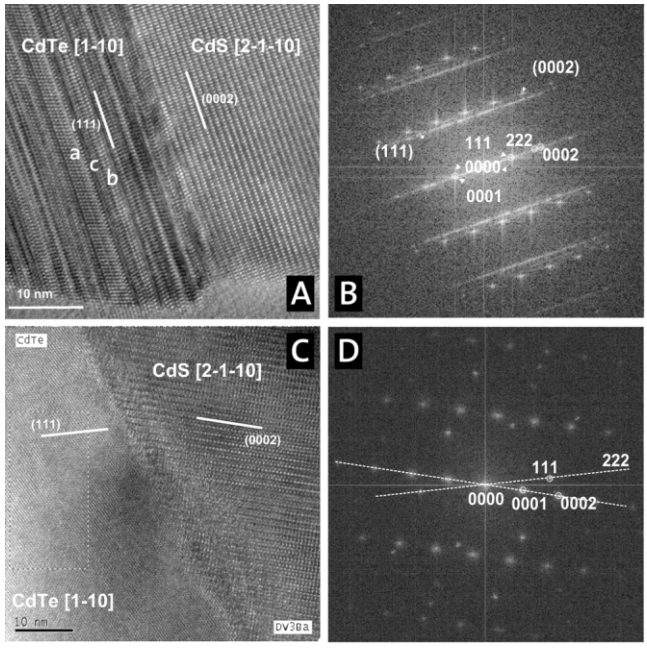

Fig. 1. High-resolution micrographs of the CdTe/CdS interface (a) before and (c) after $CdCl_2$-treatment and (b and d) the corresponding fast Fourier transforms. In the CdTe layer, (a and b) the cubic and (c) the hexagonal stacking sequence are marked.

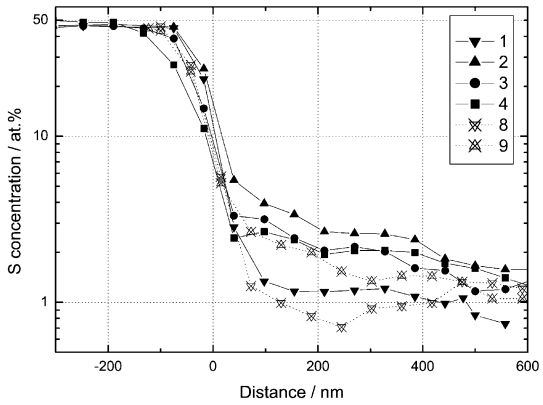

Fig. 2. Concentration profiles of sulfur across the CdTe/CdS interface for both HVE- and CSS-grown cells after deposition and after treatment with different amounts of $CdCl_2$.

reduction in defect density are less pronounced. This can be explained by the higher ratio in grain volume to defect density in CSS grown samples compared to HVE grown CdTe cells.

3.2. Chemical changes

To assess the intermixing of CdTe and CdS during the $CdCl_2$ treatment, EDS maps were obtained for samples taken from cells grown by CSS and HVE at different temperatures. A region of approximately $1.5\times1.5\ \mu m^2$ in size was scanned with a lateral resolution of 10 nm. The alignment of the interface parallel to the electron beam is crucial and was optimized by tilting the interface in the microscope until EDS line scans showed a minimum extension of the interface. Thickness effects were avoided by measuring intensity ratios between different elements. These ratios were then converted to absolute concentrations by comparison with CdS_5Te_{45} and $CdS_{45}Te_5$ standards. For clarity, the concentrations obtained are presented as linescans across the CdTe/CdS interface, and the interfaces of the different cells are aligned with respect to each other (Fig. 2). No interdiffusion is detected after deposition of the CdTe absorber layer for cells grown at 150 and 300 °C by HVE and at 550 °C by CSS. Subsequent annealing for 30 min at ~430 °C in air without Cl leads to no detectable diffusion of S into CdTe. Cells annealed under the influence of Cl show enhanced diffusion of S, increasing with the amount of Cl applied. No further increase of S diffusion is observed for $CdCl_2$ layers thicker than 400 nm. The maximum S concentration measured at the CdTe/CdS interface is approximately 6 at.%, which is in agreement with the solubility of 6 at.% CdS in CdTe in the CdTe–CdS phase diagram [5]. No preferential segregation of S along the CdTe grain boundaries was seen, but EDS and EFTEM mappings with higher resolution will be obtained in the near future. In contrast to S, Te does not diffuse noticeably into the CdS grains. However, segregation of Cl, Te and O at the CdTe/CdS interface is found with a bias towards the CdS grain boundaries, as shown in Fig. 3. Where the elements mentioned segregate, the S map shows a depletion along the CdS grain boundaries. A precise determination of the concentrations is rather difficult owing to the large number of elements. However, the simultaneous presence of Cd, Cl, Te and O is in agreement with the reactions at 430 °C proposed by McCandless [6]

$$CdCl_2(\text{solid}) + O_2(\text{gas}) + CdTe(\text{solid}) \Leftrightarrow TeCl_2(\text{gas}) + 2CdO(\text{solid}) \quad (1)$$

X-ray photoelectron spectroscopy profiling was used to verify that the oxygen does not originate from the TCO but is absorbed from the annealing ambient.

3.3. Role of chlorine

To understand how Cl reaches the CdTe/CdS interface during the annealing, a series of HVE-grown samples were annealed for different durations. After 1 min of annealing the CdTe layer shows no change. After 6 min of annealing, grains with arbitrary orientation with respect to the as-deposited grains start to appear. These grains grow from the top of the CdTe layer towards the CdTe/CdS interface, as shown in the inset of Fig. 4.

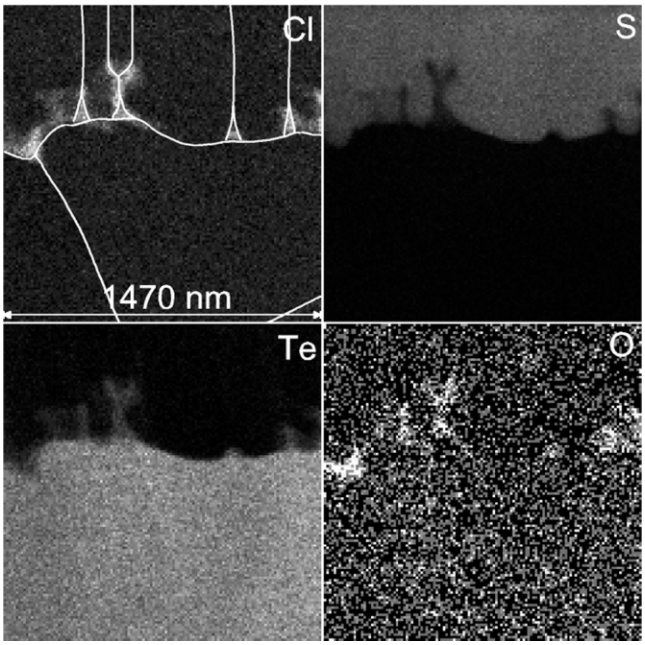

Fig. 3. EDS mappings of the CdTe/CdS interfacial region. At the interface and along the CdS grain boundaries the concentration of Te, Cl and O is higher. In the Cl map, the grains are outlined along the boundaries for clarity.

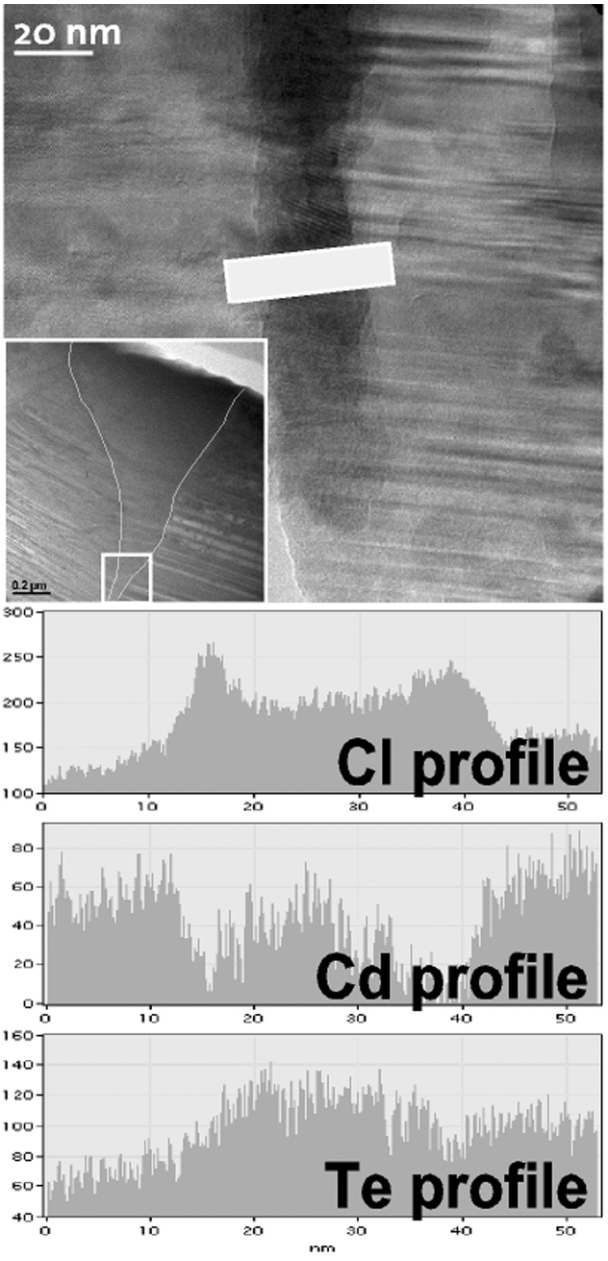

Fig. 4. Grey-scale image of a grain growing from the top of the CdTe layer towards the CdTe/CdS interface during $CdCl_2$ treatment. The white bar marks the area where the signal intensity profiles in a.u. of Cl, Cd and Te were derived from the corresponding EFTEM images. The inset shows the entire grain and its location at the top of the CdTe layer. The grain boundaries are outlined for clarity.

This figure shows a magnification of the tip of the grain together with line profiles of the intensities of the Cl, Cd and Te signals measured with EFTEM. The scans are taken at and averaged over the area marked by the white bar in Fig. 4. At the grain boundaries, the Cd concentration is lower than within the grains. Instead, an increased Cl concentration found, while the Te signal remains almost unchanged, as expected if a $TeCl_2$ complex forms according to Eq. (1). At room temperature $TeCl_2$ turns solid. In the bulk grain, both the Cd and the Te signals resume the approximate intensities measured in the adjacent as-deposited grains. The new grain shows an increased Cl concentration. After 11 min of annealing, the CdTe absorber layer is completely recrystallized, and first changes in the CdS layer become visible. The remaining Cl that has not diffused to the interface, accumulates at the CdTe grain boundaries. Fig. 5 shows an EFTEM map of a CdTe grain boundary after recrystallization with the corresponding line profile of the Cl signal measured in the white region marked in the map.

4. Conclusions

The diffusion of S during $CdCl_2$ treatment of CdTe/CdS thin film cells has been studied quantitatively, and a concentration of 6 at.% of S has been found at the

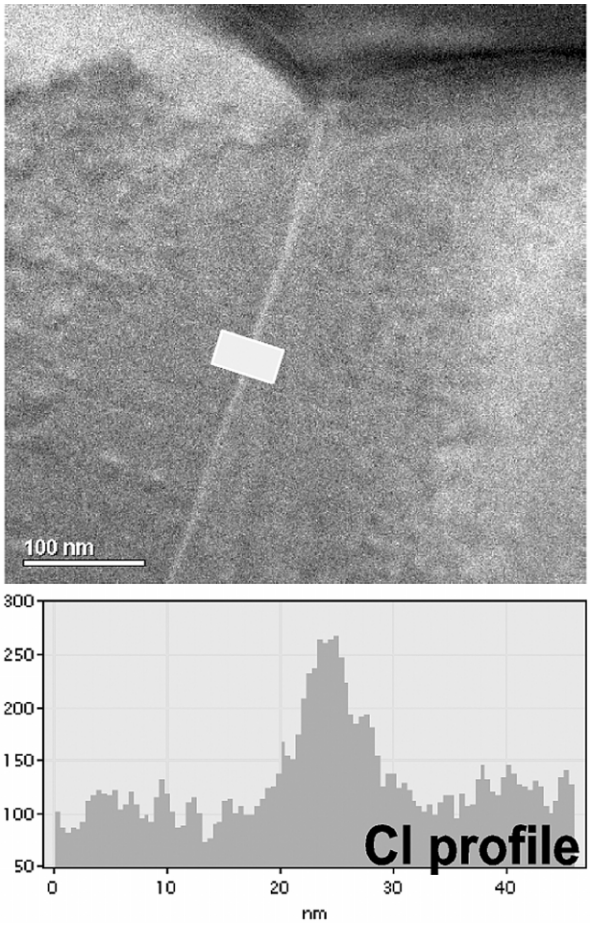

Fig. 5. An EFTEM image and the corresponding Cl signal intensity profile in a.u. averaged over the white area. The $CdCl_2$ treatment was stopped after 11 min. Segregation of Cl along CdTe grain boundaries is revealed.

interface. In contrast, no Te diffusion was detected. For the first time, a direct imaging of Cl diffusion along CdTe grain boundaries is presented. The spatial distribution of Cl, Cd, Te and O at the CdTe/CdS interface was mapped. The results suggest that the recrystallization of HVE-grown CdTe during annealing starts from the CdTe surface. The growth of these grains is favored by the formation of a gaseous $TeCl_2$ phase at the grain boundaries, as this phase enhances the mobility of Cd and Te atoms. The random orientation of CdTe grains observed after $CdCl_2$ treatment is a result of recrystallization. By this recrystallization, most of the final absorber layer is brought into good contact to Cl, and a homogeneous doping with Cl becomes possible.

References

[1] M. Harr, D. Bonnet, in: R. McNelis, W. Pals, H. Ossenbrink, P. Helm (Eds.), Proceedings of the 17th European Photovoltaic Solar Energy Conference and Exhibition, Munich, Germany, October 22–26, 2001, p. 1001.
[2] K. Durose, P.R. Edwards, D.P. Halliday, J. Crystal Growth 197 (1999) 733.
[3] G. Agostinelli, D.L. Baetzner, M. Burgelman, Thin Solid Films 431–432 (2003) 407–413.
[4] H.R. Moutinho, M.M. Al-Jassim, D.H. Levi, P.C. Dippo, L.L. Kazmerski, J. Vac. Sci. Technol. A 16 (3) (1998) 1251.
[5] D.W. Lane, G.J. Conibeer, D.A. Wood, K.D. Rogers, P. Capper, S. Romani, S. Hearne, J. Crystal Growth 197 (1999) 743.
[6] B.E. McCandless, in: R. Noufi, R.W. Birkmire, D. Lincot, H.W. Schock (Eds.), II–VI Compound Semiconductor Photovoltaic Materials, San Francisco, USA, April 16–20, 2001, Mater. Res. Soc. Symp. Proc. 668 (2001) H1.6.1.